Geophysical Research Letters

RESEARCH LETTER
10.1029/2019GL085989

Rapid Export of Waters Formed by Convection Near the Irminger Sea's Western Boundary

I. A.-A. Le Bras[1], F. Straneo[1], J. Holte[1], M. F. de Jong[2], and N. P. Holliday[3]

[1]Scripps Institution of Oceanography, University of California San Diego, La Jolla, CA, USA, [2]NIOZ Royal Netherlands Institute for Sea Research and Utrecht University, Texel, the Netherlands, [3]National Oceanography Centre, Southampton, UK

Key Points:
- From 2014 to 2016, two modes of intermediate water were formed by convection in the Irminger Sea
- Waters formed by convection near the boundary are exported more effectively by the boundary current than those formed in the basin interior
- The subduction of intermediate water into the boundary current is consistent with an eddy transport mechanism

Supporting Information:
- Supporting Information S1

Correspondence to:
I. A.-A. Le Bras,
ilebras@ucsd.edu

Citation:
Le Bras, I. A.-A., Straneo, F., Holte, J., de Jong, M. F., & Holliday, N. P. (2020). Rapid export of waters formed by convection near the Irminger Sea's western boundary. *Geophysical Research Letters*, *47*, e2019GL085989. https://doi.org/10.1029/2019GL085989

Received 24 OCT 2019
Accepted 14 JAN 2020
Accepted article online 15 JAN 2020

Abstract The standard view of the overturning circulation emphasizes the role of convection, yet for waters to contribute to overturning, they must not only be transformed to higher densities but also exported equatorward. From novel mooring observations in the Irminger Sea (2014–2016), we describe two water masses that are formed by convection and show that they have different rates of export in the western boundary current. Upper Irminger Sea Intermediate Water appears to form near the boundary current and is exported rapidly within 3 months of its formation. Deep Irminger Sea Intermediate Water forms in the basin interior and is exported on longer time scales. The subduction of these waters into the boundary current is consistent with an eddy transport mechanism. Our results suggest that light intermediate waters can contribute to overturning as much as waters formed by deeper convection and that the export time scales of both project onto overturning variability.

Plain Language Summary The deep ocean can regulate the Earth's climate by storing carbon and heat. At high latitudes, waters are cooled by the atmosphere and sink, but they can only be successfully stored in the deep ocean if they are exported toward the equator. In this study, we analyze new mooring observations in the Irminger Sea to investigate the cooling and export of high-latitude waters. In addition to the well-documented waters that are cooled in the center of the Irminger Sea, we find that saltier waters are cooled near the western boundary current. Both of these water types make it into boundary current and are exported. Our observations are consistent with the dynamics of swirling eddy motions. The eddy transport process is more effective for the waters cooled near the boundary current, implying that cooling near boundary currents may be more important for the climate than has been appreciated to date.

1. Introduction

The deep limb of the Atlantic's overturning circulation is a critical component of the climate system. In the high-latitude North Atlantic, subtropical waters are transformed into the cold, fresh, carbon- and oxygen-rich waters that fill the deep ocean, where they are isolated from the atmosphere for hundreds to thousands of years (Gebbie & Huybers, 2011). Understanding the processes which govern this subduction of waters into the deep ocean is key to quantifying the ocean's uptake of heat and carbon, and, ultimately, understanding climate stability and variability on long time scales (Khatiwala et al., 2012).

North Atlantic Deep Waters are formed in high-latitude marginal seas; the densest waters are formed in the Nordic Seas, and waters formed in the Labrador and Irminger Seas occupy intermediate depths (de Jong et al., 2012; Dickson et al., 1990; Pickart, 1992; Pickart et al., 2003; Våge et al., 2008). In winter, deep convection can occur in the center of these seas, where the stratification is weakest, forming a homogeneous water mass in the gyre interior. In climate models, waters formed by this open ocean convection dominate the variability in the overturning circulation's deep limb (Danabasoglu et al., 2016; Rahmstorf et al., 2015). However, in order for waters to enter the deep ocean they must not only be transformed to higher densities but also exported equatorward (Spall & Pickart, 2001).

Idealized modeling studies suggest that waters formed by convection are transported into boundary currents by eddies (Brüggemann et al., 2017; Georgiou et al., 2019; Spall, 2004, 2010a, 2010b, 2011; Straneo, 2006; Waldman et al., 2018). Convection steepens isopycnal gradients, which promotes eddy formation through baroclinic instability (Visbeck et al., 1996). The resulting relatively warm boundary current eddies restratify

the basin after convection (de Jong et al., 2014; Katsman et al., 2004; Lilly et al., 2003; Richards & Straneo, 2015). In order to compensate, eddy fluxes from the interior must cool the boundary current. The net result is that the boundary current becomes denser, which leads to overturning in density space (Brüggemann & Katsman, 2019; Spall, 2004; Straneo, 2006). Observations confirm that high-latitude boundary currents become denser (colder) as they circulate around marginal seas (Holte & Straneo, 2017; Mauritzen, 1996a; Pickart & Spall, 2007; Våge et al., 2013), but the processes which contribute to this density change have yet to be observed in detail.

In addition to boundary current cooling through eddy exchange with the interior, it has been hypothesized that boundary currents can be cooled directly. In the Nordic Seas, the boundary current is gradually cooled directly by the atmosphere (Isachsen et al., 2007; Mauritzen, 1996a, 1996b; Våge et al., 2013). In the Labrador Sea, Pickart et al. (1997) hypothesized that convection in the western boundary current forms a water mass called "upper Labrador Sea Water," in contrast with the denser "deep Labrador Sea Water," which is formed by deep convection in the interior. Upper Labrador Sea Water has been identified in mixed layers and subsurface eddies from winter hydrographic sections (Cuny et al., 2005; Pickart et al., 1996, 2002; Spall & Pickart, 2001) and through its high concentration of chlorofluorocarbons (Kieke et al., 2006; Stramma et al., 2004).

The Irminger Sea is thought to be similar to the Labrador Sea: Deep convection can occur in the basin interior, forming a dense convective water mass (de Jong et al., 2012; Pickart et al., 2003). In this study, we present the first observations of a light mode of convective waters, analogous to upper Labrador Sea Water, formed in the Irminger Sea. Our observations are consistent with the subduction of both light and dense convective water masses into the boundary current via an eddy transport mechanism. This process may also be relevant to the Labrador Sea.

Our study site is the western Irminger Sea, where OSNAP (Overturning in the Subpolar North Atlantic) and OOI (Ocean Observatories Initiative) moorings were simultaneously deployed starting in the summer of 2014 (Figure 1). The following winter was anomalously cold throughout the subpolar gyre, and record mixed layer depths of 1,400 m were observed in the Irminger Sea (de Jong & de Steur, 2016). The western boundary current of the Irminger Sea at this latitude is the East Greenland-Irminger Current (EGIC), which carries waters of Polar- and Atlantic-origin (Daniault et al., 2011; Le Bras et al., 2018; Pickart et al., 2005; Våge et al., 2011). From 2 years of mooring observations (summer 2014–2016), we introduce two water mass types formed by convection in the Irminger Sea (section 3.1). The lighter mode, upper Irminger Sea Intermediate Water (uISIW), appears to be formed at the edge of the boundary current, whereas the denser mode, deep Irminger Sea Intermediate Waters (dISIW), is formed in the basin interior. Though our water mass definitions overlap with others in the region, we define them to facilitate our process-based analysis, and to highlight the fact that they are formed in the Irminger Sea; the prefixes upper and deep were chosen as these water masses are analogous to upper and deep Labrador Sea Water.

Our analysis suggests that upper ISIW is subducted into the boundary current core and exported within three months of formation (section 3.2). Deep ISIW is subducted into the boundary current less effectively and, as it can be stored in the interior, its export in the boundary current may lag its formation by more than 1 year. Our observations are consistent with an eddy transport mechanism: Layer thickness anomalies propagate down-gradient into the boundary current and θ-S properties are homogenized within the upper ISIW layer (section 3.3). The implications of this study for the scientific understanding of overturning structure and variability are discussed in section 4.

2. Data and Methods

The primary data sources used in this study are a set of OSNAP and OOI moorings southeast of Greenland at about 60°N from August 2014 to July 2016 (Figure 1). Our focus is on the CF5, CF6, and M1 moorings, which are part of the United States and UK OSNAP array. These moorings include subsurface point CTD and current meter measurements, which are separated vertically by several hundred meters (Figure 1d). The shallowest recovered instruments ranged from 30 to 100 m. On CF5 and CF6, upward looking ADCPs measured velocities in the top 100 m of the water column. All OSNAP moorings were routinely blown down about 100 m, particularly CF5 and CF6, which are in the boundary current (EGIC) core. Data from the CF7 mooring, which is between CF6 and M1, were not used in this study because of a conductivity sensor failure on its 500 m instrument. The boundary between upper and deep ISIW is not as well resolved at CF6

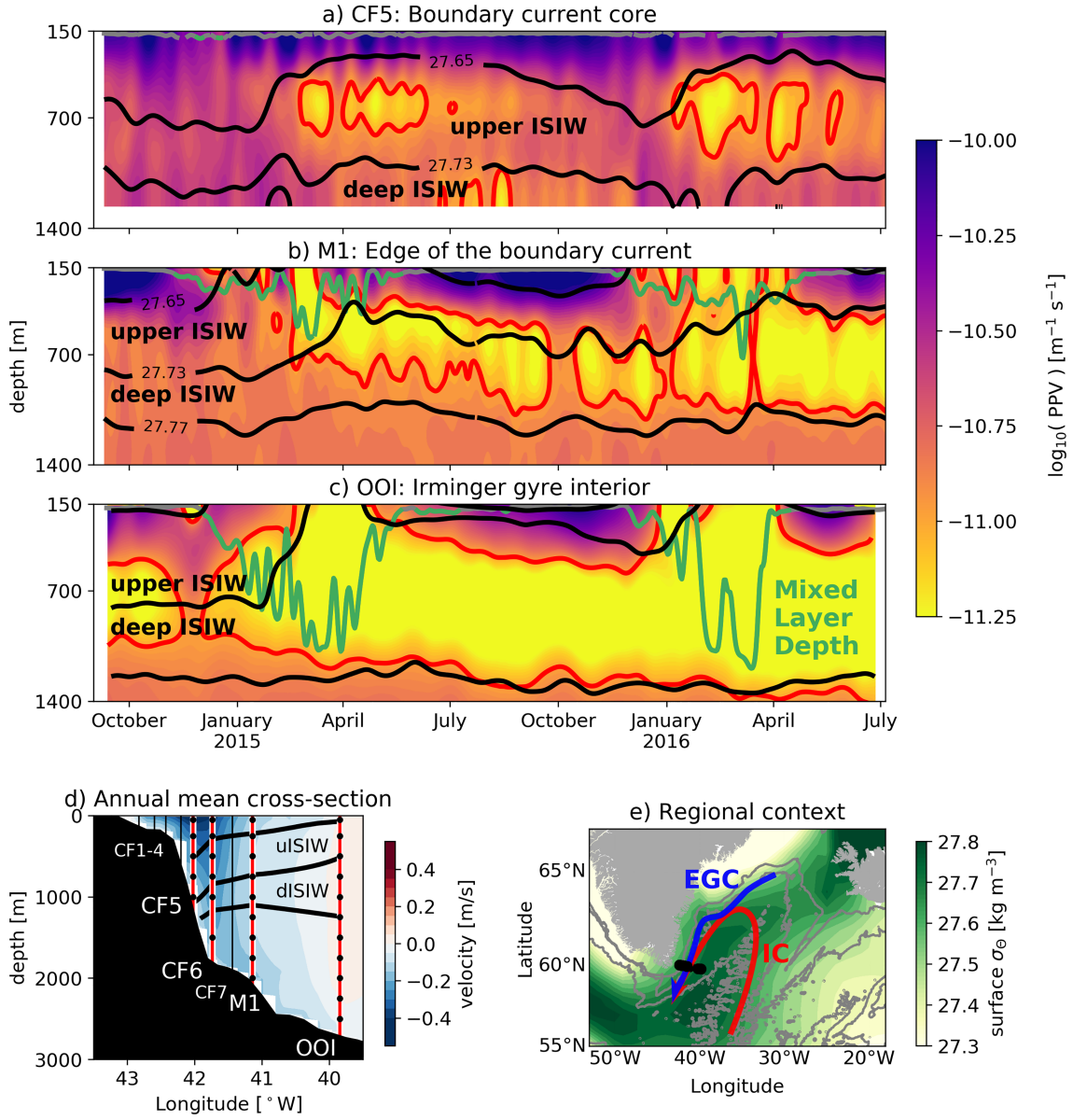

Figure 1. (a–c) Planetary Potential Vorticity (PPV) at moorings (a) within the boundary current core, (b) at the edge of the boundary current, and (c) in the interior of the Irminger gyre. Black lines indicate the isopycnals that bound upper and deep Irminger Sea Intermediate Water (ISIW; σ_θ = 27.65, 27.73, 27.77), and red contours highlight low PPV waters ($<10^{-11}$ m^{-1} s^{-1}). Green lines denote mixed layer depths; gray portions indicate that mixed layers are likely shallower than 150 m. In the boundary current core (CF5), seasonal pulses of low PPV are apparent below the local mixed layer depth within the upper ISIW density range. The winter mixed layers at the M1 mooring consistently ventilate the upper ISIW layer; the deepest mixed layers at the OOI mooring ventilate the deep ISIW layer. (d) Annual mean (August 2014–2015) cross-track velocities and density structure (Lozier et al., 2019, their Figure 2a), shown with mooring locations. The primary moorings used in this study are highlighted in red and include nominal θ-S and velocity instrument positions. (e) Map of the study region, with mooring locations in black, and winter surface density (January-March, 2015 and 2016) in the background. Bathymetry is shown in 1,000 m intervals. The western boundary current is a combination of the Polar-origin East Greenland Current (EGC) and subtropical Atlantic-origin Irminger Current (IC).

as at CF5, so it has been left out of Figure 1. Additional OSNAP mooring details, including calibration and interpolation methods, are described in Le Bras et al. (2018).

The OOI Irminger Sea global node consists of four moorings. The two subsurface flanking moorings, FLMA and FLMB, lie along the OSNAP line, and host point CTD instruments (de Jong et al., 2018). A surface mooring (SUMO), and a profiling mooring (HYPM) were deployed north of the OSNAP line, about 25 km from both flanking moorings. Unless stated otherwise, all "OOI" results presented here are based on data from FLMA below 100 m, and data from SUMO above 100 m. The standard deviation of the difference between

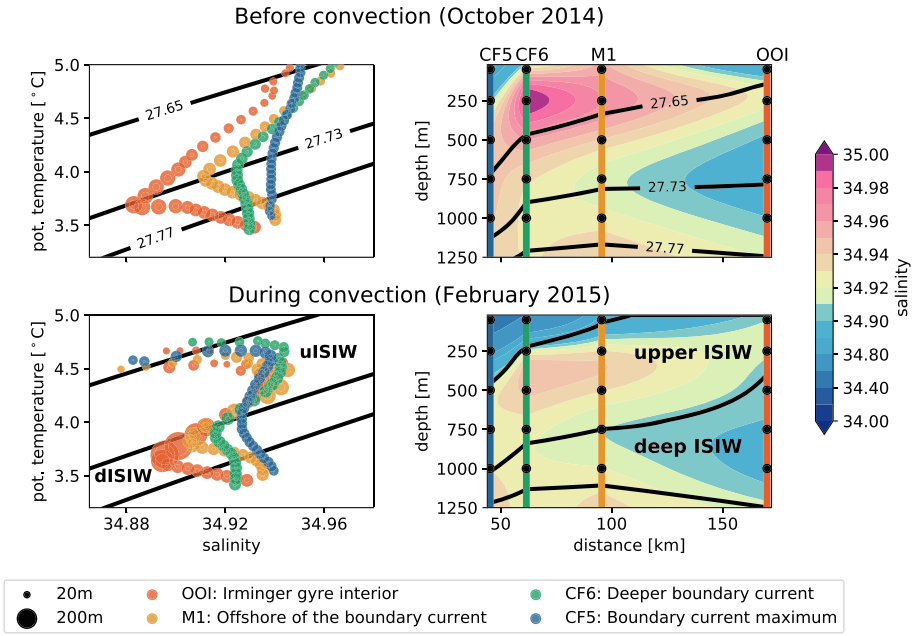

Figure 2. Monthly averaged water mass property structure before and during convection. The isopycnals that bound upper and deep ISIW are shown in each panel (σ_θ = 27.65, 27.73, 27.77). (left column) θ-S properties at each mooring. The marker size is scaled by the layer thickness of the density bin represented by each point. Before convection (October 2014), the stratification is relatively uniform and θ-S properties are distinct between moorings. During convection (February 2015), the mooring's θ-S properties converge within the upper and deep ISIW layers, and thick layers (larger markers) of upper and deep ISIW are present at M1 and OOI, respectively. (right column) Salinity sections show that before convection there are significant lateral salinity gradients within the upper and deep ISIW density layers. During convection the salinity is more uniform, particularly within the upper ISIW layer.

weekly averaged 100 m density at the FLMA and SUMO moorings where they overlap from December 2015 to July 2016 is 0.01 kg/m^3, so that our combined full depth OOI mooring profiles suit the purposes of this study.

We linearly interpolate all mooring CTD data (CF5, CF6, M1, and OOI) onto the same 5 m resolution vertical grid, so that instrument positions in the water column are resolved. The mixed layer depths shown in Figure 1 are homogeneous subsurface layers which are defined as the depth at which the potential density anomaly referenced to the surface (σ_θ) exceeds the σ_θ at 150 m by more than 0.01 kg/m^3. The subsurface depth of 150 m is chosen for this definition because it is the shallowest depth which is consistently measured at each mooring. Planetary Potential Vorticity (PPV) is the contribution of stratification to the vertical component of potential vorticity. PPV = $f/\rho \quad \partial\rho/\partial z$, where f is the Coriolis parameter, and ρ is the potential density referenced to the surface in this application. PPV from the OOI moorings is calculated from HYPM, which best resolves vertical gradients (Figure 1). To calculate layer thicknesses between isopycnal levels (Figures 2 and 3), we grid the interpolated mooring data into 0.005 kg/m^3 σ_θ bins. Boundary current (EGIC) transport is defined as in Le Bras et al. (2018): transport in the along-stream direction (203.3° clockwise from north) from CF2 to M1 (Figures 1d and 4). We also show variance in the cross-stream velocity at CF5, CF6, M1, and OOI velocity measurements at a nominal depth of 500 m recording every hour at M1 and OOI and every 30 min at CF5 and CF6 (we subsample to 1 hr to enable comparison, Figure 3c). All smoothed fields are filtered using a second-order butterworth filter. PPV and salinity are smoothed in the vertical with a 250 m cutoff (Figure 1). When filtering in time, we use a 5 day cutoff for mixed layer depth, 10 days for PPV and layer thickness, 20 days for isopycnal position and velocity variance, and 30 days for transport.

Mean winter surface density during our study period (January-March, 2015 and 2016) is from the 1° resolution EN4 monthly objective analysis, which incorporates all available temperature and salinity profile data (Figure 1e; Good et al., 2013).

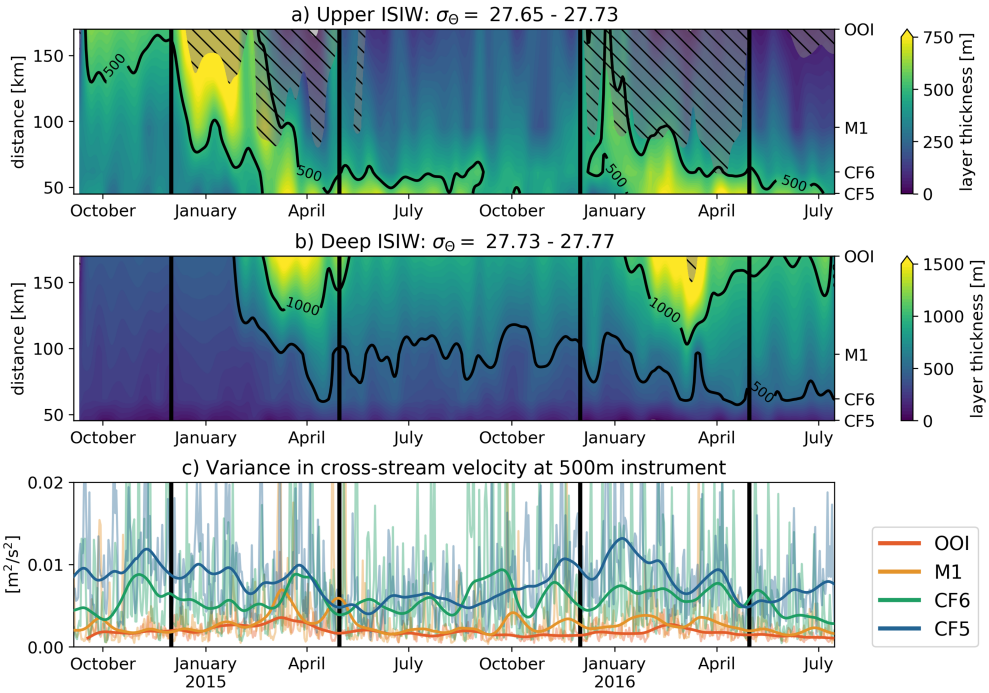

Figure 3. (a, b) Layer thickness evolution of (a) upper and (b) deep ISIW across the moored array. Distance from the shore is indicated on the left *y* axis, and mooring positions on the right. Hatched areas indicate that the full density range is not sampled, that is, that the density layer has outcropped. (a) Thick upper ISIW layers propagate into the boundary current each year within 3 months. (b) Though there is seasonal and interannual thickening of the deep ISIW layer in the boundary current, the thickest layers are found in the interior of the basin year-round. (c) Rolling variance in 24 hr windows of cross-stream velocity from instruments nominally at 500 m. Thin lines are daily averages, and bold lines are low-pass filtered. Variance is higher within the boundary current (CF5, CF6) than offshore (M1,OOI). Black vertical lines highlight the December-April time period in both years.

3. Results

3.1. Formation of Distinct Upper and Deep ISIW Water Masses

In winter 2014–2015, persistent ~1,000 m deep mixed layers were observed in the central Irminger Sea (de Jong & de Steur, 2016; de Jong et al., 2018; Piron et al., 2017). We reproduce this result and find that the low PPV (low stratification) waters formed by convection in the central Irminger Sea remain in the water column at OOI after winter 2014–2015 (Figure 1c). Closer to the boundary current, at the M1 mooring, mixed layers intermittently reach depths of 750 m in both winters (Figure 1b). The waters formed in these mixed layers at M1, at the edge of the boundary current, similarly have a low PPV signature characteristic of waters formed by convection.

We define the waters formed at the edge of the boundary current (M1) and in the central Irminger Sea (OOI) as two different water masses because they have distinct θ-S properties (Figure 2, bottom left). Upper ISIW is a local salinity maximum, and deep ISIW is a local salinity minimum. Both water masses are local modes in θ-S space: In February 2015 there are thick layers of upper ISIW at M1, and thick layers of deep ISIW at OOI.

Our definitions of upper and deep ISIW are based on the maximum winter mixed layer depths at M1 and OOI, as well as the observed modes in θ-S space. Upper and deep ISIW correspond to potential density anomaly ranges of σ_θ = 27.65–27.73 kg/m^3 and σ_θ = 27.73–27.77 kg/m^3, respectively. Note that these ranges, though lighter, overlap significantly with accepted upper and deep Labrador Sea Water density ranges (σ_θ = 27.68–27.74 and 27.74–27.8 kg/m^3; Pickart et al., 1997; Rhein et al., 2015). Our density-based definitions facilitate the discussion of the isopycnal subduction of these water masses into the boundary current.

3.2. Arrival of ISIW in the Boundary Current

In the boundary current (CF5, Figure 1a), we observe seasonal pulses of low PPV waters below the mixed layer. Hence, we conclude that these low PPV waters are not ventilated vertically within the boundary current core. Instead, we hypothesize that these low PPV waters in the upper ISIW layer are subducted into the

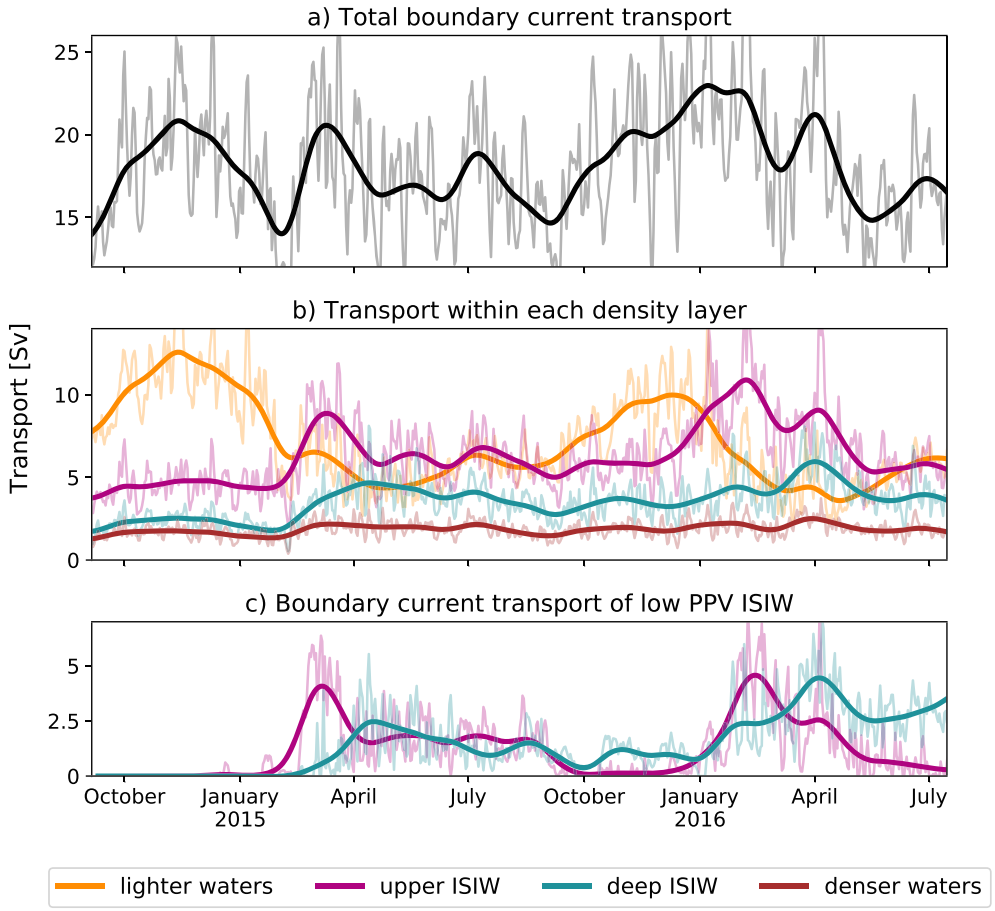

Figure 4. Volume transport time series: Thin lines are daily values and bold lines are low-pass filtered. (a) Total transport in the boundary current (EGIC; Le Bras et al., 2018). (b) Boundary current transport decomposed into density layers. (c) Transport of boundary current waters in the ISIW density ranges with PPV less than 10^{-11} m^{-1} s^{-1} (red contours in Figure 1).

boundary current from their formation sites just offshore. There are also low PPV waters in the deep ISIW layer at CF5, but these are limited by the bathymetry.

There are several indications that the low PPV waters we observe in the boundary current have an offshore source. The boundary current θ-S properties match the offshore properties in the upper ISIW density layer during convection in February 2015. Before the onset of convection, the θ-S properties in the boundary current are distinct from those offshore; there are horizontal salinity gradients within the upper and deep ISIW layers (Figure 2, top row). In February 2015, the salinity is more uniform within the upper ISIW layer (Figure 2, bottom row). The subtropical Atlantic-origin salinity maximum has been diluted through mixing with fresh, cold surface waters and is centered in the upper ISIW density layer. The changes in deep ISIW properties are less pronounced. We also observe the shoreward propagation of upper ISIW layer thickness anomalies (i.e., low PPV anomalies) in both years, from January to April (Figure 3a). The deep ISIW layer thickness anomalies do not propagate into the boundary current as coherently (Figure 3b). There is a general thickening of the deep ISIW layer throughout the domain, but it is thickest in the gyre interior throughout the year.

We decompose the boundary current transport into density classes to quantify how the arrival of ISIW into boundary current may project onto changes in overturning. From September to January, the boundary current transport is dominated by waters lighter than ISIW (in the overturning circulation's upper limb), whereas from February to August upper ISIW density classes (in the lower limb) dominate the transport (Figure 4b), that is, a larger portion of the boundary current is in the lower limb of the overturning circulation in winter. From 2014 to 2016, the boundary current transports about twice as much upper ISIW as deep

ISIW (Figure 4b), both because there is a larger area of upper ISIW in the boundary current, and because velocities are faster within the upper ISIW layer. In winter, the transport in the upper and deep ISIW layers increase by about 6 and 3 Sv, respectively. These transport increases are due both to layer thickness increases (Figure 3), and shoaling to depths where velocities are faster (Figure 2). The geostrophic shear between CF5 and CF6 increases in winter due to steepening isopycnals, however the resulting transport increase is not significant relative to the total boundary current transport variability. Barotropic velocities dominate the boundary current transport, particularly between CF6 and M1 (not shown).

To assess the boundary current export of newly ventilated ISIW, we quantify the transport of low PPV waters within the ISIW density classes (Figure 4c). In the fall of 2014, there is no low PPV ISIW in the boundary current (also apparent in Figure 1). The boundary current transport of low PPV upper ISIW peaks in both winters and returns to zero afterward, while the transport of low PPV deep ISIW almost doubles from winter 2014–2015 to winter 2015–2016, and remains elevated at the end of this record. This indicates that the water masses have different time scales of export from their formation sites: low PPV upper ISIW is completely subducted, exported, or mixed away within a year of its formation, while a reservoir of low PPV deep ISIW may remain in the basin, and can be exported over longer time scales (Figure 3b). While interpretation of this pattern is limited by the length of our record, the implication is that these two water masses may imprint on overturning variability at different time scales. Formation of upper ISIW can project onto time scales as short as seasonal, while deep ISIW projects onto a smoothed, interannual variability because it can be stored in the basin interior.

3.3. Eddy Transport Mechanism

The propagation of upper ISIW layer thickness anomalies into the boundary current is suggestive of an eddy transport mechanism (Figure 3a). Rhines and Holland (1979) showed that anomalies from the time mean, also called eddies, tend to flatten gradients of potential vorticity. A simplified version of this result is that eddies tend to relax gradients of layer thickness (Gent & McWilliams, 1990). In other words, the net effect of eddies, or high-frequency motions, is to move mass along isopycnals from areas with thicker layers to adjacent areas with thinner layers such that their thicknesses even out.

Early in the winter, offshore formation of a thick upper ISIW layer leads to a cross-shore layer thickness gradient (Figure 3a). In the subsequent months, this layer thickness gradient is relaxed, which is consistent with an eddy transport mechanism. One would expect that this transport is facilitated by enhanced eddy activity in the winter, when isopycnals are steep. Indeed, the high-frequency variance in the cross-stream velocity within the boundary current is somewhat elevated in winter (CF5 and CF6 in Figure 3c), but the signal is complicated by instrument motion and is not conclusive. There is not a significant seasonal cycle in variance at M1 or OOI. We do find that the variance in the cross-stream velocity is higher at CF5 and CF6 than at M1 an OOI; there is a more vigorous eddy field within the boundary current than in the basin interior.

The approximate across-stream propagation speed of upper ISIW layer thickness anomalies into the boundary current in the winter is 0.5 cm/s (50 km in 3 months), but we observe it within a boundary current system. Hence, this interpretation rests on the assumption that the processes we observe also occur upstream. After the initial arrival of thick upper ISIW layers in February, anomalously thick layers of upper ISIW remain in the boundary current through August (Figure 3a). Based on the fact that low PPV waters continue arriving about 4 months after production has ceased at our array, and using a mean velocity of 10 cm/s, upper ISIW is likely produced all along the edge of the boundary current, up to about 1,000 km upstream, that is, all along the path of the Irminger Current. As winter surface densities are uniform along the circulation pathways of the Irminger Sea (Figure 1e), this is a sensible hypothesis. Argo profiles are too sparse to reliably diagnose the upper ISIW formation region, but mixed layer densities from Holte et al. (2017) are broadly consistent with upper ISIW formation along the boundary of the Irminger Sea from 2014–2016 (Figure S1). It is also conceivable that upper ISIW is formed in the northern Irminger Sea, away from the boundary; however these waters would not enter the boundary current as easily.

We find that deep ISIW is subducted into the boundary current less effectively than upper ISIW: the θ-S properties in the deep ISIW layer are not as homogeneous, and a cross-shore layer thickness gradient remains in the deep ISIW layer year-round. This is consistent with our proposed mechanism, as deep ISIW is formed farther from the boundary current, where there is less variance in the velocity field (decreasing variance from CF5 to OOI, Figure 3c). Additionally, because the deep ISIW density range sits deeper in the water

column than upper ISIW, and the boundary current flows above the continental slope, there are parts of the boundary current that are confined to depths shallower than where deep ISIW occurs (Figures 1e and 3a). The proximity to the continental slope may also suppress eddy activity in the deep ISIW layer. Finally, unlike upper ISIW, which we hypothesize is formed all along the edge of the boundary current, deep ISIW is thought to be formed primarily in the southern Irminger Sea (Figures 1e and S1; Pickart et al., 2003; Piron et al., 2017). Additional deep ISIW may enter the boundary current downstream.

Our observations of the subduction of convectively formed waters into the boundary current are consistent with an eddy transport mechanism. Winter-time convection creates thick homogeneous layers offshore of the boundary current core, setting up cross-shore layer thickness gradients (Figure 3). Eddies act to relax these layer thickness gradients and transport waters shoreward along isopycnals. We find that this process is more effective in the upper ISIW layer than the deep ISIW layer, as upper ISIW is closer to the boundary current core, higher in the water column, and within a more energetic eddy field.

4. Conclusions

In this study, we investigated the interaction of convection and boundary currents using novel OSNAP and OOI mooring observations in the western Irminger Sea from 2014 to 2016. We aimed to elucidate the processes that govern the export of waters formed by convection, and define the role of convection near the boundary, given that overturning is governed by the densification of boundary currents.

Our observations suggest that the boundary current export of waters formed by convection is mediated by eddy dynamics. Convection offshore of the boundary current creates thick layers of homogeneous density, which sets up a cross-shore layer thickness gradient. We observed the shoreward propagation of layer thickness anomalies (Figure 3), and cross-shore homogenization of θ-S properties (Figure 2), consistent with the tendency of eddies to relax layer thickness gradients, and homogenize water mass properties. However, the vertical resolution of our data limits our ability to quantify the eddy transports and their associated diffusivity ($v^* = \overline{v'h'}/\bar{h}, \kappa = \overline{v'h'}/\overline{h_y}$; e.g., Marshall & Radko, 2003). Additionally, the subsurface OSNAP moorings are blown down by strong flows, and the instrument motion further complicates the interpretation of higher-frequency data.

From 2014 to 2016, we found that convection occurred at the edge of the western Irminger Sea boundary current, not within its core (Figure 1). The upper ISIW formed near the current is a local salinity maximum corresponding to ventilated subtropical Atlantic-origin water. The deep ISIW formed in the basin interior is a local salinity minimum with a θ-S signature similar to Labrador Sea Water. We find that upper ISIW is more effectively subducted into the boundary current than deep ISIW. This is likely because it is formed closer to the boundary current, within a more vigorous eddy field (Figure 3c).

Our finding that waters formed by convection are entrained into the Irminger Sea boundary current within several months are consistent with some, more limited, observations in the Labrador Sea. Rhein et al. (2015), Yashayaev and Loder (2016), Holte and Straneo (2017), and Le Bras et al. (2017) found that interannual property changes in the Labrador Current mirror those in the central Labrador Sea. Yashayaev and Loder (2016) further suggest that this correspondence holds for seasonal variability, which points to rapid entrainment into the boundary current. However, Yashayaev and Loder (2016) were not able to identify whether the waters were formed in the basin interior or within the boundary current, as we did in this study. Our results are consistent with Brandt et al. (2007), who found that Labrador Sea Water formed near the boundary current is exported more rapidly than Labrador Sea Water formed in the basin interior in a model of the subpolar North Atlantic.

Both upper and deep ISIW can be considered part of the lower limb of the overturning circulation as they lie below the isopycnal of maximum overturning (σ_θ= 27.53 and 27.66 kg/m^3 for OSNAP East and the full array, respectively; Lozier et al., 2019). Given that the boundary current transports about twice the amount of upper ISIW than deep ISIW from 2014 to 2016 (Figure 4b), we suggest that light intermediate waters such as upper ISIW are a significant component of the overturning circulation. Furthermore, as these two water masses have different export time scales, they likely project onto overturning variability in different ways. As upper ISIW appears to be exported within a year of its formation, it can have a seasonal signature, whereas deep ISIW transport may reflect smooth interannual changes and incorporate a lag, since it can be stored in the interior from year to year.

The variability that we observe in the western Irminger Sea is only one component of the full overturning variability, however, and recirculations and retroflections (e.g., Holliday et al., 2007; Lavender et al., 2000) complicate this interpretation. The intermediate waters of the Irminger Sea are lighter than those formed in the Labrador Sea and are likely transformed further before they are exported from the subpolar gyre. Decomposing the contributions of all boundary currents to cross-basin overturning in density space is the subject of future work.

Eddy dynamics feature prominently in the Southern Ocean overturning literature (e.g., Marshall & Radko, 2003; Thompson et al., 2014). However, the role of eddies in Atlantic overturning is rarely discussed outside of modeling studies (e.g., Brüggemann & Katsman, 2019; Spall, 2004; Straneo, 2006). We presented observational evidence in support of the idea that eddies mediate the export of waters formed by convection in the subpolar North Atlantic, and that eddy dynamics facilitate the export of waters formed near boundary currents in particular. We anticipate that the ongoing OSNAP and OOI observations will continue to re-shape our view of overturning in the subpolar North Atlantic.

Acknowledgments
We gratefully acknowledge the U.S. National Science Foundation: This work was supported by Grants OCE-1258823 and OCE-1756272. M. F. d J. was supported by NIOZ and EU Horizon 2020 project Blue-Action (Grant 727852). N. P. H. was supported by NERC program UK OSNAP (NE/K010875/1), UK OSNAP-Decade (NE/T00858X/1), and ACSIS (National Capability). The U.S. Cape Farewell OSNAP data reported here are available from this site (doi: 10.7924/r4fb50z9b). The UK data are available here (doi:10.5285/8c232969-11cd-3e52-e053-6c86abc07963). OOI data were obtained from the NSF Ocean Observatories Initiative Data Portal, http://ooinet.oceanobservatories.org, downloaded on 9 August 2017. EN4 data were downloaded from https://www.metoffice.gov.uk/hadobs/en4/download-en4-2-1.html on 26 October 2018. The Argo float mixed layer climatology shown in the supporting information is described in Holte et al. (2017) and was downloaded from mixedlayer.ucsd.edu on 20 November 2019. We thank M. Spall, R. Pickart, and A. Pacini for helpful scientific discussions, and F. Li and M.S. Lozier for providing the gridded velocity field across the OSNAP line (doi:10.7924/r4z60gf0f). The data presented in this manuscript would not have come about without the hard work of the entire OSNAP team, especially all scientists, technical staff, and crew who went to sea to collect these data.

References

Brandt, P., Funk, A., Czeschel, L., Eden, C., & Böning, C. W. (2007). Ventilation and transformation of labrador sea water and its rapid export in the deep Labrador current. *Journal of Physical Oceanography*, *37*, 946–961. https://doi.org/10.1175/JPO3044.1

Brüggemann, N., & Katsman, C. A. (2019). Dynamics of downwelling in an eddying marginal sea: Contrasting the Eulerian and the isopycnal perspective. *Journal of Physical Oceanography*, *49*, 3017–3035. https://doi.org/10.1175/jpo-d-19-0090.1

Brüggemann, N., Katsman, C. A., & Dijkstra, H. A. (2017). On the vorticity dynamics of the downwelling branch of the AMOC. *CLIVAR Exchanges Special Issue: CLIVAR Open Science Conference Award Winners*, *71*, 10–12.

Cuny, J., Rhines, P. B., Schott, F., & Lazier, J. (2005). Convection above the Labrador Continental Slope. *Journal of Physical Oceanography*, *35*, 489–511.

Danabasoglu, G., Yeager, S. G., Kim, W. M., Behrens, E., Bentsen, M., Bi, D., et al. (2016). North Atlantic simulations in coordinated ocean-ice reference experiments phase II (CORE-II). Part II: Inter-annual to decadal variability. *Ocean Modelling*, *97*, 65–90. https://doi.org/10.1016/j.ocemod.2015.11.007

Daniault, N., Lherminier, P., & Mercier, H. (2011). Circulation and transport at the southeast tip of Greenland. *Journal of Physical Oceanography*, *41*, 437–457. https://doi.org/10.1175/2010JPO4428.1

de Jong, M. F., Bower, A. S., & Furey, H. H. (2014). Two years of observations of warm-core anticyclones in the Labrador Sea and their seasonal cycle in heat and salt stratification. *Journal of Physical Oceanography*, *44*, 427–444. https://doi.org/10.1175/JPO-D-13-070.1

de Jong, M. F., & de Steur, L. (2016). Strong winter cooling over the Irminger Sea in winter 2014-2015, exceptional deep convection, and the emergence of anomalously low SST. *Geophysical Research Letters*, *43*, 7106–7113. https://doi.org/10.1002/2016GL069596

de Jong, M. F., Oltmanns, M., Karstensen, J., & De Steur, L. (2018). Deep convection in the Irminger Sea observed with a dense mooring array. *Oceanography*, *31(1)*, 50–59. https://doi.org/10.5670/oceanog.2018.109

de Jong, M. F., Van Aken, H. M., Våge, K., & Pickart, R. S. (2012). Convective mixing in the central Irminger Sea: 2002-2010. *Deep-Sea Research Part I: Oceanographic Research Papers*, *63*, 36–51. https://doi.org/10.1016/j.dsr.2012.01.003

Dickson, R. R., Gmitrowicz, E. M., & Watson, A. J. (1990). Deep-water renewal in the northern North Atlantic. *Nature*, *344*, 848–850.

Gebbie, G., & Huybers, P. (2011). How is the ocean filled? *Geophysical Research Letters*, *38*, L06604. https://doi.org/10.1029/2011GL046769

Gent, P. R., & McWilliams, J. C. (1990). Isopycnal mixing in ocean circulation models. *Journal of Physical Oceanography*, *20*, 150–155. https://doi.org/10.1175/1520-0485(1990)020<0150:imiocm>2.0.co;2

Georgiou, S., van der Boog, C. G., Brüggemann, N., Ypma, S. L., Pietrzak, J. D., & Katsman, C. A. (2019). On the interplay between downwelling, deep convection and mesoscale eddies in the Labrador Sea. *Ocean Modelling*, *135*, 56–70. https://doi.org/10.1016/J.OCEMOD.2019.02.004

Good, S. A., Martin, M. J., & Rayner, N. A. (2013). EN4: Quality controlled ocean temperature and salinity profiles and monthly objective analyses with uncertainty estimates. *Journal of Geophysical Research: Oceans*, *118*, 6704–6716. https://doi.org/10.1002/2013JC009067

Holliday, N. P., Bacon, S., Alderson, S. G., Cuevas, B. D., Meyer, A., Bacon, S., et al. (2007). Retroflection of part of the east Greenland current at Cape Farewell. *Geophysical Research Letters*, *34*, L07609. https://doi.org/10.1029/2006GL029085

Holte, J., & Straneo, F. (2017). Seasonal overturning of the Labrador Sea as observed by Argo floats. *Journal of Physical Oceanography*, *47*, 2531–2543. https://doi.org/10.1175/JPO-D-17-0051.1

Holte, J., Talley, L. D., Gilson, J., & Roemmich, D. (2017). An Argo mixed layer climatology and database. *Geophysical Research Letters*, *44*, 5618–5626. https://doi.org/10.1002/2017GL073426

Isachsen, P. E., Mauritzen, C., & Svendsen, H. (2007). Dense water formation in the Nordic Seas diagnosed from sea surface buoyancy fluxes. *Deep Sea Research Part I: Oceanographic Research Papers*, *54*, 22–41. https://doi.org/10.1016/J.DSR.2006.09.008

Katsman, C. A., Spall, M. A., & Pickart, R. S. (2004). Boundary current eddies and their role in the restratification of the Labrador Sea. *Journal of Physical Oceanography*, *34*, 1967–1983. https://doi.org/10.1175/1520-0485(2004)034<1967:bceatr>2.0.co;2

Khatiwala, S., Primeau, F., & Holzer, M. (2012). Ventilation of the deep ocean constrained with tracer observations and implications for radiocarbon estimates of ideal mean age. *Earth and Planetary Science Letters*, *325-326*, 116–125.

Kieke, D., Rhein, M., Stramma, L., Smethie, W. M., LeBel, D. A., & Zenk, W. (2006). Changes in the CFC inventories and formation rates of upper Labrador Sea water, 1997–2001. *Journal of Physical Oceanography*, *36*, 64–86. https://doi.org/10.1175/JPO2814.1

Lavender, K. L., Davis, R. E., & Owens, W. B. (2000). Mid-depth recirculation observed in the interior Labrador and Irminger seas by direct velocity measurements. *Nature*, *407*, 66–96.

Le Bras, I. A., Straneo, F., Holte, J., & Holliday, N. P. (2018). Seasonality of freshwater in the East Greenland current system from 2014 to 2016. *Journal of Geophysical Research: Oceans*, *123*, 8828–8848. https://doi.org/10.1029/2018JC014511

Le Bras, I. A., Yashayaev, I., Toole, J. M., & 5348–5366 (2017). Tracking Labrador Sea water property signals along the deep western boundary current. *Journal of Geophysical Research: Oceans*, *122*, 5348-5366. https://doi.org/10.1002//2017JC012921

Lilly, J. M., Rhines, P. B., Schott, F., Lavender, K., Lazier, J., Send, U., & D'Asaro, E. (2003). Observations of the Labrador Sea eddy field. *Progress in Oceanography*, *59*, 75–176. https://doi.org/10.1016/J.POCEAN.2003.08.013

Lozier, M. S., Li, F., Bacon, S., Bahr, F., Bower, A. S., Cunningham, S. A., et al. (2019). A sea change in our view of overturning in the subpolar North Atlantic. *Science (New York, N.Y.)*, *363*, 516–521. https://doi.org/10.1126/science.aau6592

Marshall, J., & Radko, T. (2003). Residual-mean solutions for the Antarctic Circumpolar Current and its associated overturning circulation. *Journal of Physical Oceanography*, *33*, 2341–2354. https://doi.org/10.1175/1520-0485(2003)033<2341:RSFTAC>2.0.CO;2

Mauritzen, C. (1996a). Production of dense overflow waters feeding the North Atlantic across the Greenland-Scotland Ridge. Part 1: Evidence for a revised circulation scheme. *Deep-Sea Research Part I: Oceanographic Research Papers*, *43*, 769–806. https://doi.org/10.1016/0967-0637(96)00037-4

Mauritzen, C. (1996b). Production of dense overflow waters feeding the North Atlantic across the Greenland-Scotland Ridge. Part 2: An inverse model. *Deep Sea Research Part I: Oceanographic Research Papers*, *43*, 807–835. https://doi.org/10.1016/0967-0637(96)00038-6

Pickart, R. S. (1992). Water mass components of the North Atlantic deep western boundary current. *Deep-Sea Research*, *39*, 1553–1572.

Pickart, R. S., Smethie, W. M., Lazier, J. R. N., Jones, E. P., & Jenkins, W. J. (1996). Eddies of newly formed upper Labrador Sea water. *Journal of Geophysical Research*, *101*, 20,711–20,726. https://doi.org/10.1029/96JC01453

Pickart, R. S., & Spall, M. A. (2007). Impact of Labrador Sea convection on the North Atlantic Meridional Overturning Circulation. *Journal of Physical Oceanography*, *37*, 2207–2227. https://doi.org/10.1175/JPO3178.1

Pickart, R. S., Spall, M. A., & Lazier, JohnRN (1997). Mid-depth ventilation in the western boundary current system of the sub-polar gyre. *Deep Sea Research Part I: Oceanographic Research Papers*, *44*, 1025–1054.

Pickart, R. S., Straneo, F., & Moore, G. W. K (2003). Is Labrador Sea water formed in the Irminger basin?. *Deep Sea Research Part I: Oceanographic Research Papers*, *50*, 23–52. https://doi.org/10.1016/S0967-0637(02)00134-6

Pickart, R. S., Torres, D. J., & Clarke, R. A. (2002). Hydrography of the Labrador Sea during active convection. *Journal of Physical Oceanography*, *32*, 428–457. https://doi.org/10.1175/1520-0485(2002)032<0428:hotlsd>2.0.co;2

Pickart, R. S., Torres, D. J., & Fratantoni, P. S. (2005). The East Greenland spill jet. *Journal of Physical Oceanography*, *35*, 1037–1053.

Piron, A., Thierry, V., Mercier, H., & Caniaux, G. (2017). Gyre-scale deep convection in the subpolar North Atlantic Ocean during winter 2014-2015. *Geophysical Research Letters*, *44*, 1439–1447. https://doi.org/10.1002/2016GL071895

Rahmstorf, S., Box, J. E., Feulner, G., Mann, M. E., Robinson, A., Rutherford, S., & Schaffernicht, E. J. (2015). Exceptional twentieth-century slowdown in Atlantic Ocean overturning circulation. *Nature Climate Change*, *5*, 1–6. https://doi.org/10.1038/nclimate2554

Rhein, M., Kieke, D., & Steinfeldt, R. (2015). Advection of North Atlantic deep water from the Labrador Sea to the Southern Hemisphere. *Journal of Geophysical Research: Oceans*, *120*, 1–17. https://doi.org/10.1002/2014JC010605.Received

Rhines, P. B., & Holland, W. R. (1979). A theoretical discussion of eddy-driven mean flows. *Dynamics of Atmospheres and Oceans*, *3*, 289–325.

Richards, C. G., & Straneo, F. (2015). Observations of water mass transformation and eddies in the Lofoten Basin of the Nordic Seas. *Journal of Physical Oceanography*, *45*, 1735–1756. https://doi.org/10.1175/JPO-D-14-0238.1

Spall, M. A. (2004). Boundary currents and watermass transformation in marginal seas. *Journal of Physical Oceanography*, *34*, 1197–1213. https://doi.org/10.1175/1520-0485(2004)034<1197:BCAWTI>2.0.CO;2

Spall, M. A. (2010a). Dynamics of downwelling in an eddy-resolving convective basin. *Journal of Physical Oceanography*, *40*, 2341–2347. https://doi.org/10.1175/2010JPO4465.1

Spall, M. A. (2010b). Non-local topographic influences on deep convection: An idealized model for the Nordic Seas. *Ocean Modelling*, *32*, 72–85. https://doi.org/10.1016/J.OCEMOD.2009.10.009

Spall, M. A. (2011). On the role of eddies and surface forcing in the heat transport and overturning circulation in marginal seas. *Journal of Climate*, *24*, 4844–4858. https://doi.org/10.1175/2011JCLI4130.1

Spall, M. A., & Pickart, R. S. (2001). Where does dense water sink? A subpolar gyre example. *Journal of Physical Oceanography*, *31*, 810–826. https://doi.org/10.1175/1520-0485(2001)031<0810:WDDWSA>2.0.CO;2

Stramma, L., Kieke, D., Rhein, M., Schott, F., Yashayaev, I., & Koltermann, K. P. (2004). Deep water changes at the western boundary of the subpolar North Atlantic during 1996 to 2001. *Deep Sea Research I*, *51*, 1033–1056. https://doi.org/10.1016/j.dsr.2004.04.001

Straneo, F. (2006). On the connection between dense water formation, overturning, and poleward heat transport in a convective basin. *Journal of Physical Oceanography*, *36*, 1822–1840. https://doi.org/10.1175/JPO2932.1

Thompson, A. F., Heywood, K. J., Schmidtko, S., & Stewart, A. L. (2014). Eddy transport as a key component of the Antarctic overturning circulation. *Nature Geoscience*, *7*, 879–884. https://doi.org/10.1038/ngeo2289

Våge, K., Pickart, R. S., Moore, G. W. K., & Ribergaard, M. H. (2008). Winter mixed layer development in the central Irminger Sea: The effect of strong, intermittent wind events. *Journal of Physical Oceanography*, *38*, 541–565. https://doi.org/10.1175/2007JPO3678.1

Våge, K., Pickart, R. S., Sarafanov, A., Knutsen, Ø., Mercier, H., Lherminier, P., et al. (2011). The Irminger Gyre: Circulation, convection, and interannual variability. *Deep-Sea Research Part I: Oceanographic Research Papers*, *58*, 590–614. https://doi.org/10.1016/j.dsr.2011.03.001

Våge, K., Pickart, R. S., Spall, M. a., Moore, G. WK, Valdimarsson, H., Torres, D. J., et al. (2013). Revised circulation scheme north of the Denmark Strait. *Deep-Sea Research Part I: Oceanographic Research Papers*, *79*, 20–39. https://doi.org/10.1016/j.dsr.2013.05.007

Visbeck, M., Marshall, J., & Jones, H. (1996). Dynamics of isolated convective regions in the ocean. *Journal of Physical Oceanography*, *26*, 1721–1734. https://doi.org/10.1175/1520-0485(1996)026<1721:DOICRI>2.0.CO;2

Waldman, R., Brüggemann, N., Bosse, A., Spall, M., Somot, S., & Sevault, F. (2018). Overturning the Mediterranean thermohaline circulation. *Geophysical Research Letters*, *45*, 8407–8415. https://doi.org/10.1029/2018GL078502

Yashayaev, I., & Loder, J. W. (2016). Recurrent replenishment of Labrador Sea water and associated decadal-scale variability. *Journal of Geophysical Research: Oceans*, *121*, 8095–8114. https://doi.org/10.1002/2016JC012046